Synthetic Metals 161 (2011) 2259–2267

Contents lists available at SciVerse ScienceDirect

Synthetic Metals

journal homepage: www.elsevier.com/locate/synmet

Mechanical characterizations of cast Poly(3,4-ethylenedioxythiophene):Poly(styrenesulfonate)/Polyvinyl Alcohol thin films

Chang-hsiu Chen[a,*], Anna Torrents[b], Lawrence Kulinsky[b], Richard D. Nelson[c], Marc J. Madou[a,b,d,e], Lorenzo Valdevit[a,b], John C. LaRue[b]

[a] Department of Chemical Engineering & Materials Science, University of California, Irvine, CA 92697, United States
[b] Department of Mechanical & Aerospace Engineering, University of California, Irvine, CA 92697, United States
[c] Department of Electrical Engineering & Computer Science, University of California, Irvine, CA 92697, United States
[d] Department of Biomedical Engineering, University of California, Irvine, CA 92697, United States
[e] UNIST, World Class University (WCU), Ulsan, South Korea

ARTICLE INFO

Article history:
Received 11 June 2011
Received in revised form 18 August 2011
Accepted 20 August 2011
Available online 17 September 2011

Keywords:
PEDOT
PEDT
PVA
Polyvinyl Alcohol
Conducting polymers
Young's modulus
Mechanical properties

ABSTRACT

The polymer Poly(3,4-ethylenedioxythiophene):Poly(styrenesulfonate), hereafter referred to as PEDOT:PSS, has electrical properties superior to those of most conducting polymers, but it is too brittle to be employed in many applications. Blending PEDOT:PSS with other polymers is a promising route to reach a good trade-off between electrical and mechanical properties. This paper describes the mechanical characterization of PEDOT:PSS/PVA (Polyvinyl Alcohol) blends. The PEDOT:PSS/PVA films used in this study are produced by casting, and uniaxial tensile tests are performed to characterize the Young's modulus, fracture strain, tensile strength, and plastic deformation behavior of the blends as a function of the weight fraction of the components. For pure PVA, the Young's modulus, fracture strain and tensile strength are found to be, respectively, 41.3 MPa, 111% and 41.3 MPa. The strength exhibits a nearly perfect bimodal behavior, suddenly increasing by a factor 2 at a PEDOT:PSS content of 30%. Importantly, the ductility remains extremely high (~94%, only 20% lower than pure PVA) up to PEDOT:PSS fractions of ~50%. The Young's modulus monotonically increases with PEDOT:PSS content, reaching 1.63 GPa at 50%. SEM imaging and XRD analysis allows correlation of these evolutions to substantial morphological changes in the PEDOT:PSS/PVA microstructure. When combined with a previously published electrical characterization study, the current work suggests that a PEDOT:PSS/PVA polymer blend with 30–40 wt% of PEDOT:PSS provides the best trade-off of conductivity and ductility. For non free-standing films, higher PEDOT:PSS fractions (70%) might be preferable.

1. Introduction

In recent years, there has been increased interest in the study of organic materials for electronic devices and Micro-Electro-Mechanical Systems (MEMS) [1–3]. Examples include organic transistors, optical amplifiers, electroluminescent devices, sensors, and switchable membranes [4–9]. Organic materials are low-cost, easy to process and compliant. These properties are ideal for the fabrication of inexpensive, foldable and flexible miniaturized devices [1–3].

Poly(3,4-ethylenedioxythiophene):Poly(styrenesulfonate) (PEDOT:PSS) is one of the most promising conducting polymers for industrial applications [10–13]. It has a high electrical conductivity in the doped state (up to 500 S/cm) as well as good thermal and chemical stability. It is a bio-compatible, easily processed and non-toxic material, which is widely used in electronic, optical, electrochemical and biomedical applications [14,15]. The electrical properties of PEDOT:PSS have been well characterized [10–13]. However, few studies of its mechanical have been published. In many applications, the performance of a system is strongly related to the level of mechanical stress in the polymeric components. Hence, knowledge of the mechanical properties of the material is essential for design optimization and fabrication of MEMS devices.

While PEDOT:PSS has a relatively high electrical conductivity, it is brittle and, hence, difficult to form into a free-standing film. In its pure form, it has been found to have a relatively high Young's modulus and low ductility [13,16]. In this study, Polyvinyl Alcohol (PVA) is blended with PEDOT:PSS in order to enable the formation of free-standing films with a well-balanced combination of strength and ductility. PVA, a water soluble synthetic polymer, has excellent

* Corresponding author. Tel.: +1 949 824 2431; fax: +1 949 824 3732.
E-mail address: changhsc@uci.edu (C.-h. Chen).

0379-6779/$ – see front matter © 2011 Elsevier B.V. All rights reserved.
doi:10.1016/j.synthmet.2011.08.031

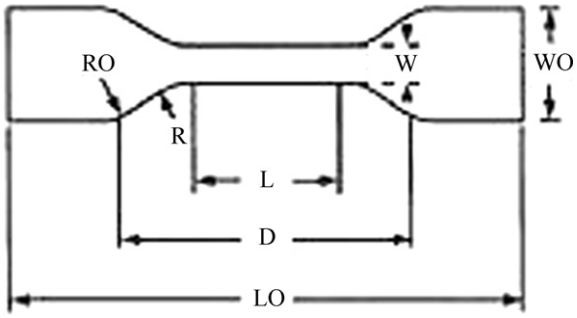

Fig. 1. Dimensions of ASTM D638 type IV specimen (W: 6 mm, L: 33 mm, WO: 19 mm, LO: 114 mm, D: 64 mm, R: 14 mm, RO: 25 mm).

film-forming, emulsifying, and adhesive properties, which make it an attractive material for many biotechnology applications [17]. The addition of PVA to PEDOT:PSS enhances the ductility, durability, and flexibility of the resulting films. However, the sulfonate groups in PSS and the hydroxyl groups in PVA easily form hydrogen bonds, reducing the negative charge in the PSS and consequently lowering the conductivity from about 1 S/cm (for pure PEDOT:PSS) to roughly 0.002 S/cm (for 20 wt% PEDOT:PSS in PEDOT:PSS/PVA blends) [18].

The present work describes the processing of conductive PEDOT:PSS/PVA films and reports on their mechanical properties for PEDOT:PSS weight fractions ranging from 0% to 50%. Uniaxial tensile tests are performed to determine the Young's modulus, tensile strength and ductility of the PEDOT:PSS/PVA blends. SEM images are obtained that show the morphology of PEDOT:PSS/PVA. X-ray diffraction studies of as-cast and *post-mortem* films are used to infer the microstructural changes that take place under large strain.

2. Experimental

2.1. Materials and synthesis

PEDOT doped with PSS is commercially available in the form of an aqueous dispersion (Clevios P v4071 from H.C. Starck GmbH, solid content 1.2%). A high conductivity formulation (CPP105D) is provided by the manufacturer [13]. PVA (98–99% hydrolyzed, Alfa Aesar, average M.W. 88,000–97,000) is dissolved in de-ionized water at 90 °C for 4 h to obtain a 9 wt% aqueous solution. The PEDOT:PSS dispersion (CPP105D formulation) and a PVA water solution are blended and stirred with a magnetically driven paddle for 24 h. They are mixed at solid weight fractions of PEDOT:PSS varying from 0% to 50%.

2.2. Films and specimen preparation

Casting is utilized to form polymer films for all the PEDOT:PSS/PVA blends used in this study. The polymer solutions corresponding to the various weight percentages of PEDOT:PSS are poured into a 150 mm-long, 100 mm-wide and 1 mm-deep open metal mold. After overnight evaporation of the solvent in air, the dry films have a thickness of 0.12 mm. All the coupons for mechanical testing are cut (with a blade) from the cast polymer films to produce ASTM D 638 type IV Dog Bone shape specimen (Fig. 1).

2.3. Mechanical testing

The mechanical properties of the PEDOT:PSS/PVA films are investigated using uniaxial tensile tests. The tests are performed using a servo-electric INSTRON 8862 frame, equipped with a FastTrack 8800 controller and a National Instrument SCXI Data Acquisition system. Conventional INSTRON mechanical tensile grips are used to clamp the specimen. The displacement rate is accurately controlled at 0.15 mm/s for all tests. The loads are measured using a 100 kN INSTRON Dynacell load cell, and the displacements are measured using an internal linear variable differential transformer (LVDT) embedded in the frame actuator. The excellent dynamic range of the load cell enabled sufficiently accurate measurements for all tests: some inconsequential noise is only observed at very small loads. Fig. 2 shows the uniaxial tensile test setup with a sample loaded. The relative humidity (rH) was held to $40 \pm 2\%$. Load–displacement relationships are constructed and true stress and true strain are calculated as described in Section 3.1. Young's moduli in the elastic region are determined following the approach described in Section 3.2. The samples are repeatedly strained and unloaded in cyclic tensile tests to evaluate the strain hardening and stiffening behavior in the plastic region, as described in Section 3.3.

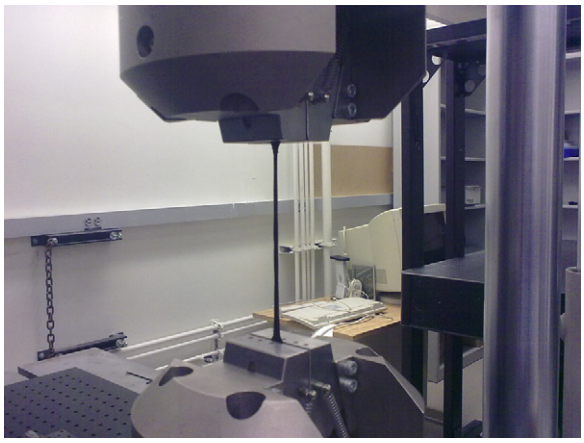

Fig. 2. Uniaxial tensile test setup.

Most polymers are viscoelastic, and exhibit a non-linear stress–strain response at large strain. In this study, large-deformation, quasi-static mechanical measurements are performed, at constant strain rate. The effects of strain rate on the mechanical properties and on the damping characteristics of the polymer are not investigated in this study.

2.4. SEM and X-ray diffraction analysis

SEM images were taken using a Philips XL-30 FEG SEM with the 10 kV electron beam with SE (secondary electron) detector. Wide-angle X-ray diffraction profiles are extracted at room temperature using a Siemens Kristalloflex Diffraktometer D5000. Diffraction patterns for all tested specimens are collected before and after tensile strength measurements to evaluate the microstructural changes that occur during uniaxial tensile testing. The X-ray diffraction study is performed for the range of 2θ angles from 10° to 90° with a scanning rate of 0.04°/s.

3. Results

In Section 3.1, the true stress and stress are defined and their values are presented for different weight percentages, allowing extraction of tensile strength and ultimate tensile strain. The approach used to determine the Young's modulus and values for the Young's modulus and tangent modulus are presented in Section 3.2, while Section 3.3 shows data representative of the large strain behavior.

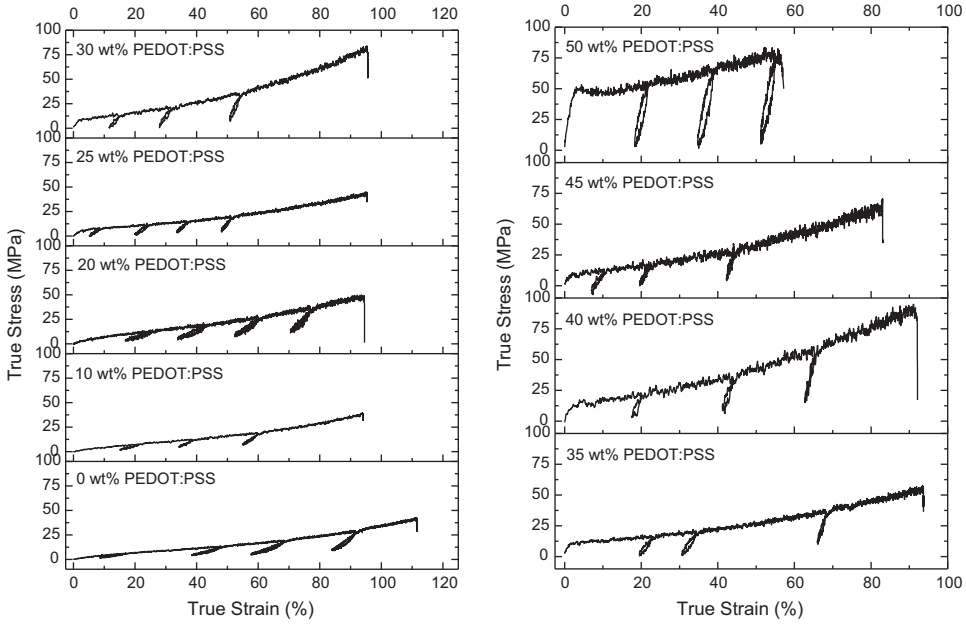

Fig. 3. True stress–strain relationships for different weight percentage of PEDOT:PSS in PEDOT:PSS/PVA blends.

3.1. Stress–strain relationships

Engineering stress (σ_e) and strain (ε_e) are directly extracted from the measured load (P) and displacement (ΔL), whereby:

$$\sigma_e = \frac{P}{A_0}$$
$$\varepsilon_e = \frac{\Delta L}{L_0} \quad (1)$$

A_0 and L_0 are, respectively, the initial cross-sectional initial area and initial length of the sample. As all samples undergo large deformations, results are presented in terms of the true stress (σ_t) and true strain (ε_t) as defined in Eq. (2) [19].

$$\sigma_t = \sigma_e(1 + \varepsilon_e)$$
$$\varepsilon_t = \ln(1 + \varepsilon_e) \quad (2)$$

The experimental true stress–true strain curves for 0 wt% (pure PVA) to 50 wt% of PEDOT:PSS in PEDOT:PSS/PVA blends are plotted in Fig. 3. A series of unload–reload cycles are performed at discrete strain intervals to track the evolution of the tangent modulus with increasing strain. It can be observed that, as is typical of many polymers, the stress is not a linear function of the strain and the nonlinearity increases with increasing weight percentage. The end of the stress–strain curves shows the percentage elongation at break and tensile strength (the maximum stress that a material can withstand before it breaks). The observed (but inconsequential) data scattering is due to the large load cell range (see Section 2.3).

Figs. 4 and 5 show the elongation at break (in %) and the tensile strength as a function of weight percentage (wt%) of PEDOT:PSS. It is evident that increasing the weight percentage of PEDOT:PSS increases the tensile strength but decreases the ductility. Consequently, the percentage elongation at break is a maximum for pure PVA. In addition, as seen in Fig. 4, the percentage elongation at break for blends with a weight percentage of 10% is about 20% lower than that of pure PVA, but it remains nearly the same up to a weight fraction of 40% and then decreases thereafter. The tensile strength, as shown in Fig. 5, remains nearly the same as that of pure PVA up to a weight percentage of 25%. Relative to the average tensile strength in the low weight percentage range, for weight percentages of 30% and higher, the tensile strength increases by about 80%, and remains

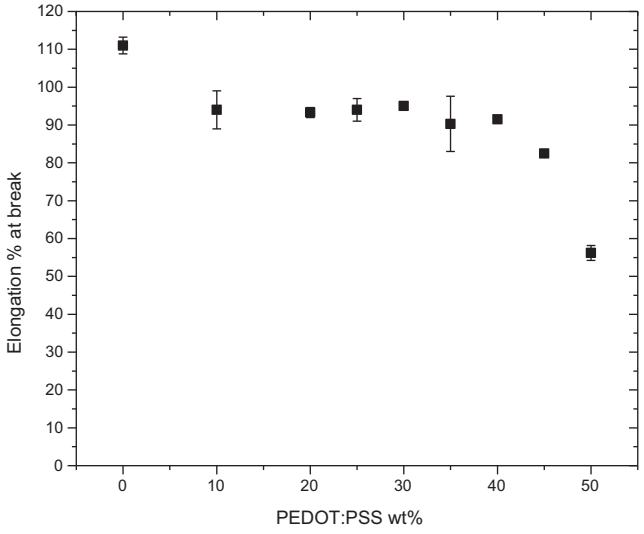

Fig. 4. Percentage elongation at break for different weight percentage of PEDOT:PSS in PEDOT:PSS/PVA blends.

roughly constant in the 30–50% range. These results suggest that a change in morphology of the sample takes place at weight percentages in the range of 25–40%. This hypothesis is further discussed in Section 4.

3.2. Determination of Young's moduli and tangent moduli at low strain levels

The Young's and tangent moduli are determined following the procedure outlined in ASTM E 111. Specifically, at low strain levels, the method of least squares is implemented using Origin 8.0 (Origin Lab) software to determine a second order polynomial that describes the true strain–true stress data in the strain range from 0% to 1.5%. Comparisons of the second order polynomial with experimental data are shown in Fig. 6. The tangent moduli are determined by differentiating the second order polynomial and evaluating that expression at different values of the strain. The Young's modulus is

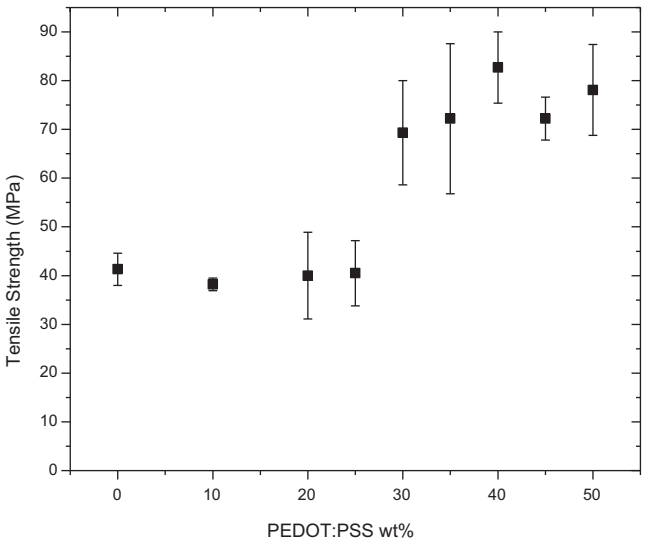

Fig. 5. Tensile strength for different weight percentage of PEDOT:PSS in PEDOT:PSS/PVA blends.

defined as the value of the tangent moduli at 0% strain. The effect of PEDOT:PSS weight fraction on the Young's modulus of the blends is reported in Fig. 7. The Young's moduli and tangent moduli at various strain levels and are also presented in Table 1.

Several samples of each weight percentage are tested and the variation in Young's modulus for the samples is indicated by the vertical line in Fig. 7(a). Humidity has been shown to have a dramatic effect on the mechanical properties of pure PEDOT:PSS [16]. For example, a change in humidity from 56% rH to 40% rH leads to a 100% change in Young's modulus. Based on a linear interpolation of the data, a ±2% rH fluctuation (typical of our laboratory) would lead to a variation of about ±12.5% in Young's modulus. The sample-to-sample variation for the 40 wt% film is about 14%. Therefore, the variation at this wt% could be due, at least in part, to fluctuations

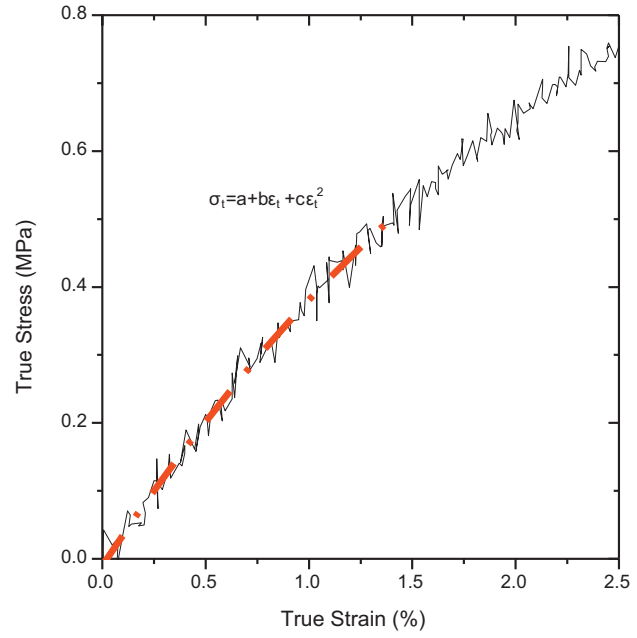

Fig. 6. Stress versus strain at low strain values for pure PVA. The solid curve shown is the second order curve fit to the stress–strain data in the range from 0% to 1.5% ($a=-9.8\times10^3$, $b=4.5\times10^7$, $c=-6.4\times10^8$).

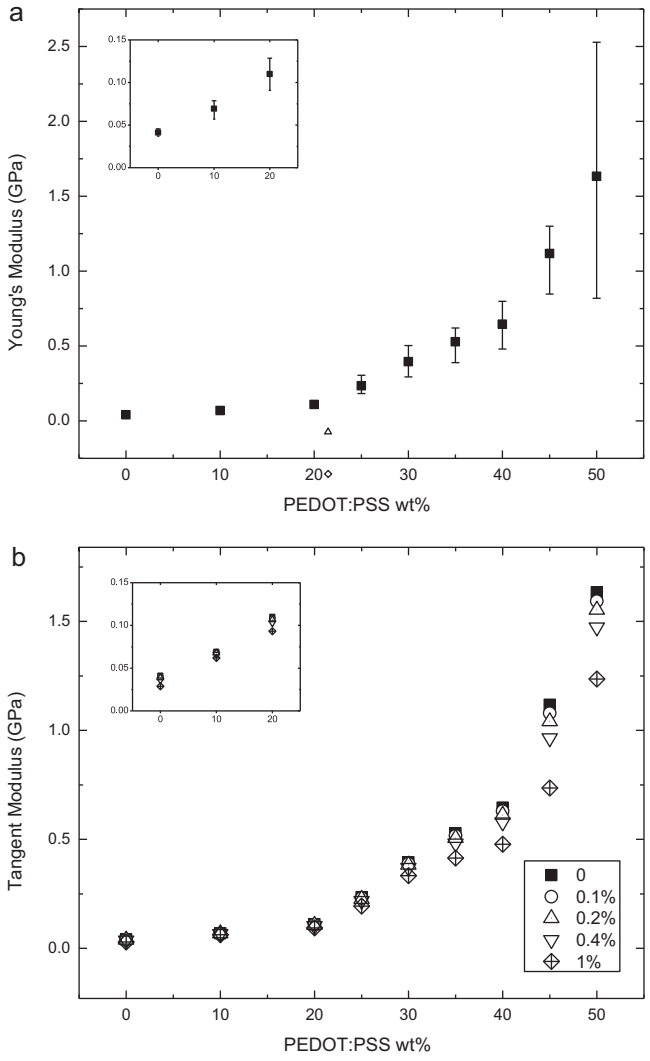

Fig. 7. (a) Young's moduli at 0% strain with variability at different strains for various weight percentages of PEDOT:PSS in PEDOT:PSS/PVA blends. (b) Young's and tangent moduli at different strains for various weight percentages of PEDOT:PSS in PEDOT:PSS/PVA blends.

in humidity level. However, it must be remembered that blends of PEDOT:PSS and PVA are the focus of the study presented herein.

Fig. 7 and Table 1 demonstrate that the Young's modulus of PEDOT:PSS/PVA blends are significantly affected by the PEDOT:PSS content. For example, increasing the PEDOT:PSS content from 0% to 50% results in a 40-fold increase in the Young's modulus from 0.0413 GPa to 1.6323 GPa. All blends show nearly linear elastic

Table 1
Young's moduli and tangent moduli (in GPa) determined from the second polynomial least squares fit to the stress–strain data at low strains.

PEDOT:PSS wt%	Strain				
	0%	0.1%	0.2%	0.4%	1%
0	0.0413	0.0400	0.0387	0.0362	0.0287
10	0.0691	0.0684	0.0677	0.0663	0.0620
20	0.1099	0.1082	0.1066	0.1032	0.0932
25	0.2346	0.2305	0.2264	0.2182	0.1936
30	0.3947	0.3886	0.3825	0.3702	0.3334
35	0.5279	0.5165	0.5051	0.4824	0.4140
40	0.6456	0.6288	0.6120	0.5783	0.4775
45	1.1171	1.0789	1.0407	0.9644	0.7351
50	1.6323	1.5926	1.5529	1.4736	1.2354

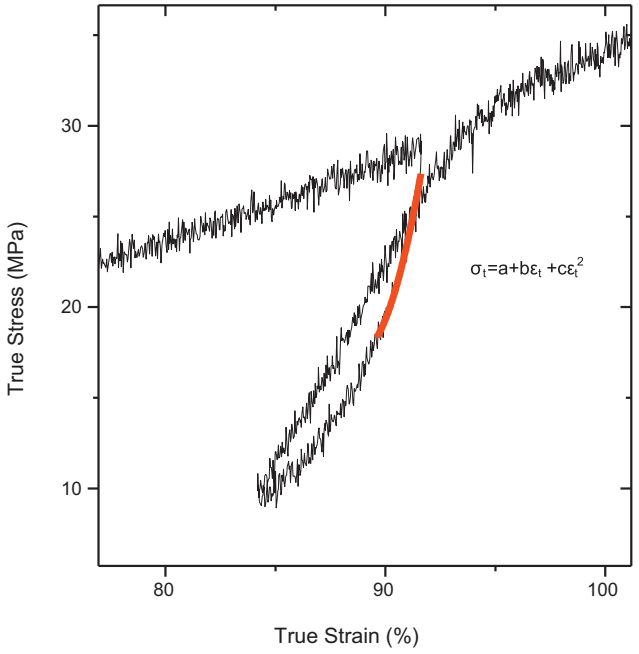

Fig. 8. Unload–reload cycle for pure PVA at an unload strain of 91.4%. The solid line corresponds to the second order least square fit in the range of strain from unload strain point to 1.5% less than the unload strain ($a=9.4\times10^9$, $b=2.1\times10^{10}$, $c=-1.1\times10^{10}$).

behavior for strains lower than 0.2%. As shown in Table 1, for all blends, in the non-linear, low strain elastic region ($0.2\%<\varepsilon\leq1\%$), the tangent modulus consistently decreases with increasing strain. It should be noted that the rate of decrease increases with increasing weight percentage. This is consistent with the viscoelastic behavior of most polymers [20].

3.3. Characterization of the large strain behavior

The results of the tensile tests shown in Fig. 3 include large strains generated under repeated unload–reload conditions. A sample of an unload–reload cycle for pure PVA at an unload strain value of 91.4% is shown in Fig. 8. To determine the tangent moduli for the unload portion of the unload–reload cycle, a second order polynomial is fit (using the method of least squares) to the data within the range the unload strain to 1.5% strain less than that the unload strain. The corresponding second order curve fit is superimposed as the solid line on the stress–strain data in Fig. 8. As is typical for all the unload–reload cycles, the data are well described by the second order polynomial. The tangent moduli as a function of the values of the strain at the unload point for all PEDOT:PSS weight fractions are shown in Fig. 9. All the blends exhibited a significant increase in the tangent modulus with increasing strain. This is attributable to PEDOT:PSS chain alignment along the loading direction, which is discussed in more detail in Section 4.

In summary, based on the results discussed in this section, the following are observed:

(i) The strength exhibits a strongly bimodal trend with PEDOT:PSS content, with a sharp nearly two-fold increase at 25–30% (Fig. 5).
(ii) The elongation at break is nearly constant for PEDOT:PSS content between 10 and 40% (Fig. 4).
(iii) The Young's modulus increases monotonically with PEDOT:PSS content, with sharp rate increases at 20% and 40% (Fig. 7).
(iv) The Young's modulus increases monotonically with strain in the large-strain region (Fig. 9).

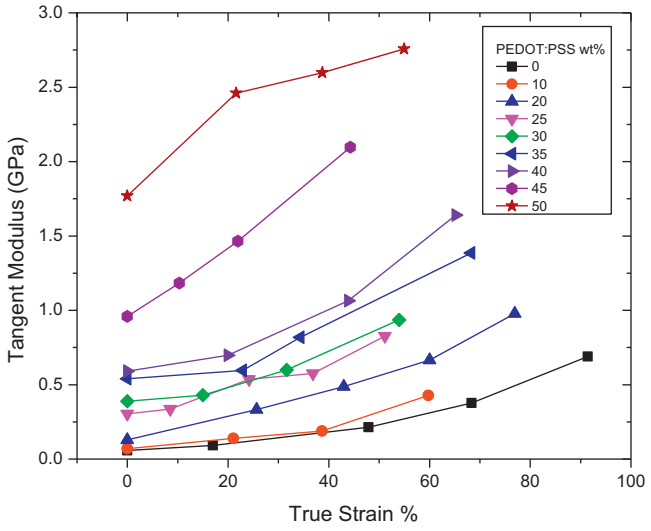

Fig. 9. Tangent moduli obtained from unload–reload cycles at different large strain values for various weight fractions of PEDOT:PSS in PEDOT:PSS/PVA blends.

4. Discussion

In Section 4.1, the Young's moduli obtained in the present study are compared with previously reported results. In Section 4.2, the key mechanical results are related to microstructural features. In Section 4.3, the variation from ductile to brittle behavior with increasing weight percentage of PEDOT:PSS is discussed. Section 4.4 discusses multifunctionality, whereby the ideal composition for eletro-mechanical applications is identified.

4.1. Comparison of Young's moduli from the present and previous studies

The Young's moduli for different weight percentages of PEDOT:PSS are shown in Fig. 7 and are presented in Table 1. In both the figure and the table, Young's modulus corresponds to the entries for 0% strain. Pure PVA (0 wt% PEDOT:PSS) is found in the present study to have a Young's modulus of 41.3 MPa and in Li et al. [21] and Strawhecker and Manias [22] to have, respectively, values of 49.5 MPa and 68.5 MPa. Taking into account the uncertainty reported in [21] and the uncertainty in the results of the present study, the results from Li et al. [21] and the present study are in reasonable agreement. However, the result from Strawhecker and Manias [22] is about 50% higher than either of the other two results. It is possible that sample preparation or environmental differences (temperature, humidity, etc.) play a role in the observed differences.

At 50 wt% PEDOT:PSS, the value of Young's modulus increases to 1.6323 GPa, i.e., by a factor of 40 relative to the Young's modulus of pure PVA. For weight fractions higher than 50%, the material becomes too brittle to allow fabrication of good-quality free standing films and, thus, results for weight fractions of higher than 50% are not reported in the present study. While we could not find mechanical property data for the PEDOT:PSS/PVA blends, Lang et al. [16] and Okuzaki and Ishihara [23] report Young's moduli of pure PEDOT:PSS between 0.9 GPa and 2.5 GPa, and the variation may well be attributed to variation in sample shape, fabrication process and humidity level. Results from the present study and the studies referenced in this section are presented in Table 2.

Table 2
Mechanical properties of PVA from the present and previous studies, pure PEDOT:PSS from previous studies and the highest weight percentage of the present study.

Material	Specimen	Young's modulus	Tensile strength	Breaking elongation	Reference
PVA	Thin film	49.5 ± 3.2 MPa	12.5 ± 0.8 MPa	265.1 ± 6.3%	[21]
PVA	Cast film	68.5 MPa	22.5 MPa	N/A	[22]
PVA	Cast film	41.3 MPa	41.3 ± 3.3 MPa	111.0 ± 2.2%	Present study
PEDOT:PSS	Pipetted film	2.8 ± 0.5 GPa (23% rH) 1.9 ± 0.02 GPa (40% rH) 0.9 ± 0.2 GPa (55% rH)	53.2 ± 9.5 MPa (23% rH) 33.7 ± 10 MPa (40% rH) 22.2 ± 4 MPa (55% rH)	N/A	[16]
PEDOT:PSS	Cast film	1.8 ± 0.2 GPa	42.8 ± 9.2 MPa	N/A	[23]
PEDOT:PSS	Fiber	1.1 ± 0.3 GPa	17.2 ± 5.1 MPa	4.3 ± 2.3%	[23]
PEDOT:PSS/PVA	Cast film	1.632 GPa (50% PEDOT:PSS)	78.1 ± 9.3 MPa (50% PEDOT:PSS)	56.2 ± 2.0% (50% PEDOT:PSS)	Present study

4.2. Relation between mechanical properties and microstructural features

This section presents the microstructural features of the polymer blends as a function of weight fraction of PEDOT:PSS.

SEM micrographs of *post-mortem* samples in the vicinity of the fracture surface are depicted in Fig. 10, for weight percentages of PEDOT:PSS of 10%, 20%, 30% and 40%. All the samples were stained using Ruthenium Tetroxide to highlight regions with PSS which appear as the brighter features in the SEM micrographs [24].

Not surprisingly, at all weight fractions, the PSS-rich areas exhibit a granular structure. As expected, the density of grains increase with increasing weight percentage of PEDOT:PSS. At weight percentages of 10–20%, a number of very small grains with a characteristic size of 100 nm or smaller can be seen. As these grains are of the same size as the manufacturer-supplied PEDOT:PSS particles [25], they are likely composed primarily of PEDOT:PSS, with little if any PVA. Also, although some clusters are present, individual clusters do not extend for more than a few microns.

At weight percentages of 30% and 40%, the size of the grains increases and few, if any, grains with a characteristic size of 100 nm or smaller are observed. Furthermore, at weight fractions larger than 30%, the grains look somewhat sintered, and seem to form a percolating network across the sample.

Another interesting microstructural feature observed at 10–20% PEDOT:PSS is the presence of irregularly shaped plate-like morphologies. Their darker rendition in the SEM micrograph suggests that these features may consist primarily of PVA. The plate-like morphologies are relatively extensive at low weight percentages, but become less so at weight percentages of 30% and nearly disappear at a weight percentage of 40%.

The appearance of a percolating network of sintered PEDOT:PSS particles at 30% weight fraction is entirely consistent with the sharp increase in the strength reported above (Fig. 5). At weight fractions less than 20%, a crack path entirely within the PVA can be easily propagated. Conversely, once a percolating network of sintered particles is established, fracture must progress by separating the sintered PEDOT:PSS particles, with resulting strength increase. Surprisingly, this two-fold strength increase is not accompanied by any reduction in ductility (Fig. 4), suggesting that the PVA matrix surrounding the clusters provides substantial toughening. The transition from disperse to percolating clusters also explains the sharp increase in the rate at which the Young's modulus varies with PEDOT:PSS content, observed at a 20% PEDOT:PSS weight fraction (Fig. 7).

As mentioned previously, for pure PEDOT:PSS grains, humidity has been shown to have a significant effect on the value of Young's modulus [16]. That study found a corresponding change

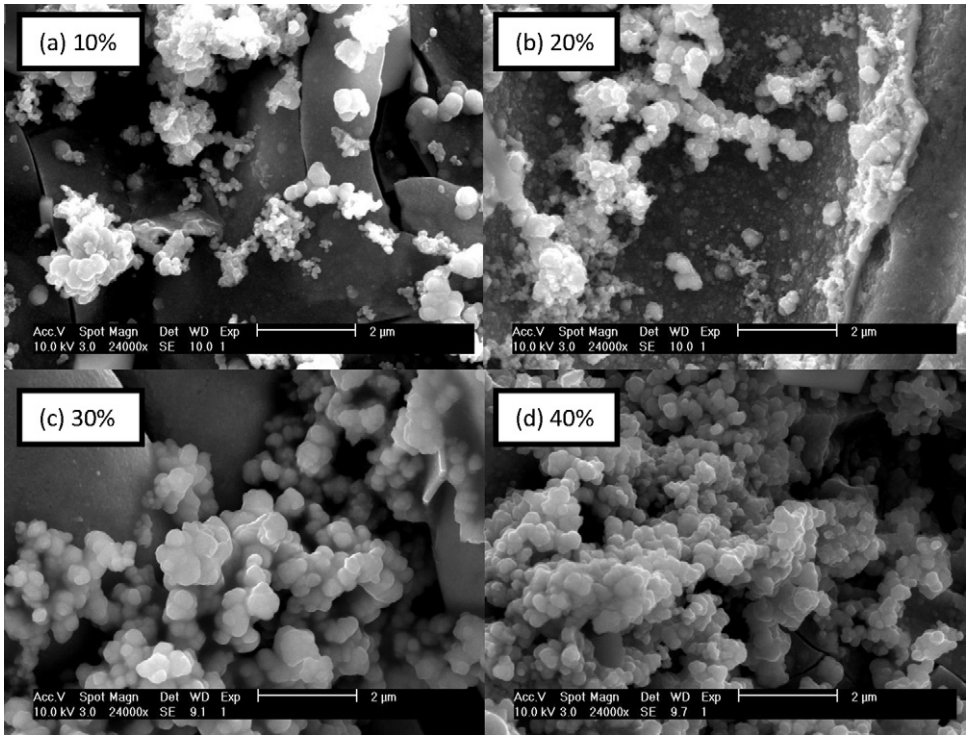

Fig. 10. SEM pictures of (a) 10%, (b) 20%, (c) 30% and (d) 40% of PEDOT:PSS in PEDOT:PSS/PVA blends.

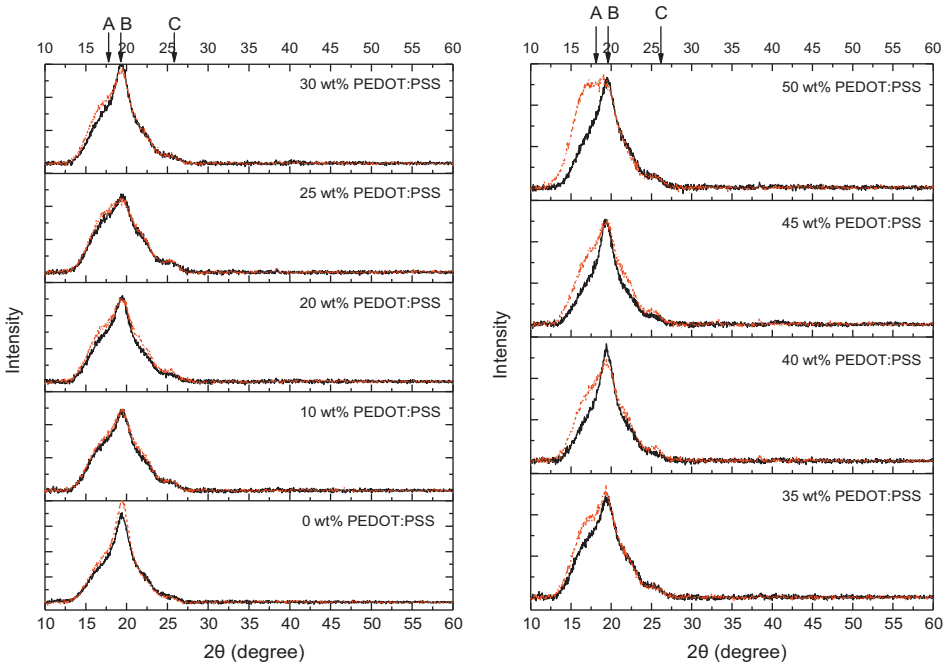

Fig. 11. X-ray diffraction scan of samples before (black solid lines) and after (red dotted lines) tensile strength measurements. (For interpretation of the references to color in this figure legend, the reader is referred to the web version of the article.)

in the failure mode from transgranular rupture at 23% rH to intergranular rupture at 40% rH. Since all the results reported herein correspond to a nominal rH of 40%, it is expected that the failure mode would be intergranular and we note that the SEM pictures are not inconsistent with this observation.

The strain stiffening behavior clearly evident at all PEDOT:PSS fractions (Fig. 9) is not surprising for a polymer. For example, similar behavior is observed for cellulose fibers [26] and standard-modulus Poly-*p*-phenylenebenzobisoxazole (PBO) fibers [27], where straining leads to an irreversible change in fiber orientation, accompanied by a pronounced increase in the elastic modulus of the specimen. At large strains, the alignment of molecular chains along the loading directions requires breaking of weaker bonds [20]. In the following we provide crystallographic evidence in support of this stiffening mechanism in the material system under consideration.

X-ray diffraction is used to characterize the molecular structure of the various blends. Fig. 11 shows the X-ray diffraction spectra for blends at different PEDOT:PSS weight percentages. The black solid line represents spectra obtained from as-cast, non-strained samples, whereas the red dotted curve represents spectra obtained from *post-mortem* samples (i.e., samples that have been strained to fracture). The strongest peak at $2\theta = 19.44^\circ$ (arrow B in Fig. 11) corresponds to the (1 0 1) plane of the semi-crystalline PVA [21,22]. With the exception of pure PVA, all blends exhibit an additional smaller peak at $2\theta = 25.8^\circ$ (arrow C in Fig. 11) which corresponds to the (0 2 0) plane of PEDOT:PSS [28,29]. In addition, the *post-mortem* data (red dotted lines in Fig. 10) show one new peak at $2\theta \sim 17.7^\circ$ (arrow A in Fig. 11), which increases in intensity with increase in weight percentage of PEDOT:PSS. This peak is attributed to the poly(styrenesulfonate) groups (most likely in the form of salts), and is confirmed by the X-ray diffraction spectrum of sodium 4-vinylbenzenesulfonate powder (Sigma Aldrich), as shown in Fig. 12. The presence of these groups in the fracture region of the post-mortem samples (in quantities roughly proportional to the PEDOT:PSS content) is surmised as follows.

PEDOT:PSS, a dark blue aqueous dispersion, commercially known as Clevios P, is the polymerized form of PEDOT in an aqueous polyelectrolyte solution (commonly PSS), with $Na_2S_2O_8$ as the oxidizing agent [13]. Bonding between PEDOT and PSS takes place through the poly(styrenesulfonate) groups of PSS. When the material is strained uniaxially in tension, polymeric chains align, inducing breaking of either PEDOT/PSS bonds and/or PEDOT:PSS/PVA bonds, in both cases exposing the poly(styrenesulfonate) groups. The exposed groups react with the water vapor in the atmosphere, and acids or salts are formed which is consistent with the formation of a peak in the XRD spectrum at $2\theta \sim 17.7^\circ$. This mechanism has been already reported in the literature: Oh et al. [30] have produced X-ray diffraction patterns for 4-styrene sulfonic acid sodium salt, exhibiting a peak at $2\theta = 17.7^\circ$, with intensity proportional to the sulfonic acid content. In the case of PEDOT:PSS/PVA blends, the amount of acids and salts formed is proportional to the number of PEDOT/PSS and PEDOT:PSS/PVA bonds. Although the peak at $2\theta \sim 17.7^\circ$ is hard to distinguish from the peak associated with PVA ($2\theta = 19.44^\circ$), its intensity clearly increases with increasing PEDOT:PSS weight percentage in the post-mortem XRD spectrum, supporting the argument presented. This provides microstructural evidence for alignment of the polymer chains, and provides a reason for the mechanical stiffening

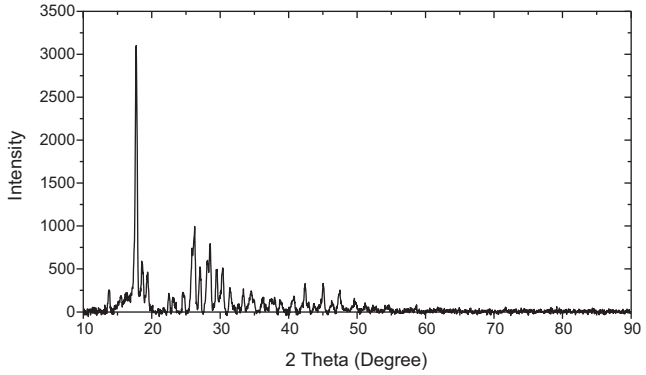

Fig. 12. X-ray diffraction pattern of sodium 4-vinylbenzenesulfonate powder, clearly indicating the $2\theta = 17.7^\circ$ peak corresponding to the poly(styrenesulfonate) group.

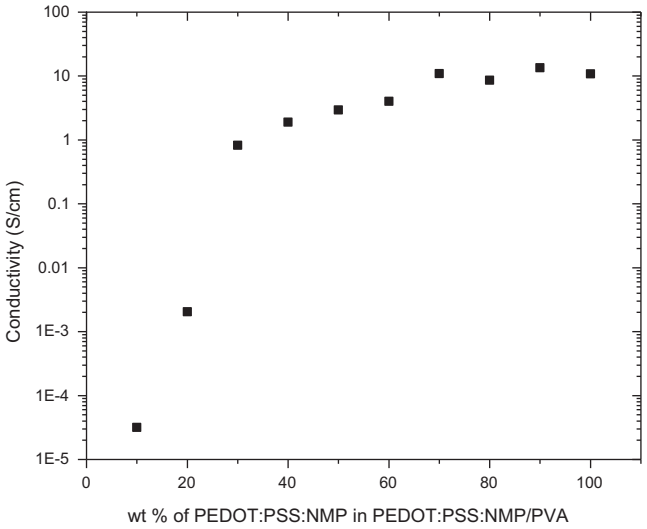

Fig. 13. Electrical conductivity as a function of wt% of PEDOT:PSS in PEDOT:PSS/PVA blends.

evident in the data of the present study. In closing, we observe that an additional mechanism might be partly responsible for the observed stiffening. As the samples are progressively strained, the PEDOT:PSS grains will pack more densely. It is reasonable to assume that this will induce stronger grain-to-grain bonding, and consequently increase the stiffness.

4.3. Brittle and ductile behavior of the PEDOT:PSS/PVA

The strains at the break point and the tensile strengths for all blends are presented in Figs. 4 and 5. It can be seen that the weight fraction of PEDOT:PSS in the blend has a strong influence on the mechanical properties of the polymer. For pure PVA, the strain at the break point is about 111%. The strain at the break point is nearly constant as weight fraction of PEDOT:PSS in the range between 10% and 40% where it is about 20% less than that of the pure PVA. The strain at the break point decreases rapidly for weight percentages of 40–50%, and at 50% the strain at the break point is only 56% of the strain at failure for the pure PVA. Thus, there is a modest decrease in ductility, corresponding to the modest decrease in strain at the break point for PEDOT:PSS weight percentages in the range of 10–35%, with a more significant reduction in ductility for weight percentages of 40% and 50%. The relatively large reduction in ductility at weight percentages of 40% and 50% is not surprising, as it is well known that pure PEDOT:PSS is a brittle material, i.e. Lang et al. [16] report a strain at failure lower than 10% strain for pure cast PEDOT:PSS). Conversely, the existence of a plateau with nearly constant ductility is an important and unexpected result. The implications of this result to the design of multifunctional films are discussed in the next section.

4.4. Electrical/mechanical properties trade-offs

The electrical properties of PEDOT:PSS/PVA have been reported previously [18]. Fig. 13 shows the dependence of the electrical conductivity on the PEDOT:PSS content. The conductivity increases sharply in the 0–30% range, which correlates well with the microstructural change from a plate-like morphology to an interconnected sintered grain morphology which percolates throughout the film. The conductivity continues to increase at a slower rate until about 65% and stabilizes thereafter. As shown above, for free-standing films, an ideal compromise of strength and ductility is achieved at ~30–40% PEDOT:PSS. At those weight percentages, the electrical conductivity is still relatively high (Fig. 13), suggesting that this composition yields optimal electro-mechanical properties for biomedical, electrochemical, and MEMS applications. For 30 and 40 wt% PEDOT:PSS, the conductivities are 0.825 and 1.89 S/cm, while the Young's moduli are 0.3947 and 0.6456 MPa, respectively. For applications requiring maximum conductivity, but where free standing films are not required, PEDOT:PSS weight percentages of 70% might be preferred (as the conductivity is around 10 S/cm).

5. Summary and conclusions

This paper presents a quasi-static mechanical characterization of PEDOT:PSS/PVA blends. The Young's modulus increases dramatically with PEDOT:PSS content, from 0.0413 GPa (pure PVA) to 1.65 GPa (50 wt% of PEDOT:PSS). A number of unload–reload cycles are performed at periodic strain increments, all the way to failure, thus allowing quantitative characterization of strain-induced stiffening. SEM images reveal a significant change in the microstructure as weight percentage increases, transitioning from a (mostly PVA) plate-like morphology with disperse clusters of PEDOT:PSS to a morphology characterized by interconnected and percolating networks of PEDOT:PSS grains. The PEDOT:PSS weight fraction for this transition (20–30%) is accompanied by a two-fold increase in strength (from 40 to 75–80 MPa) and a marked increase in the rate at which the Young's modulus varies with PEDOT:PSS content. Importantly, this morphological change seems to have no effect on the ductility of the films, which remains extremely high (~94%, only 20% lower than pure PVA). To relate the observed strain stiffening to the progressive alignment of the molecular chains upon straining, results from an X-ray diffraction study are presented. Comparison of as-cast and *post-mortem* samples reveals clear microstructural changes due to straining. Strained samples show the appearance of a X-ray diffraction peak at $2\theta = 17.7^\circ$, which is more intense at higher weight percentages of PEDOT:PSS. This peak indicates the presence of poly(styrenesulfonate) acid. As discussed, it is reasonable to attribute the acid formation to breaking of the weakest bonds in the structure upon molecular alignment with the loading direction. Data presented in this study can be used in conjunction with electrical property investigations previously reported, to determine the optimal PEDOT:PSS/PVA blend for electro-mechanical applications. Based on those data, for free standing films, a PEDOT:PSS content between 30% and 40% presents a reasonable trade-off between electrical and mechanical properties. For applications requiring maximum conductivity but where films can supported (i.e. not free-standing), PEDOT:PSS contents above 70% might be preferred.

Acknowledgements

The authors would like to thank Mingje Sung and Dr. Jianguo Zheng in The Laboratory for Electron and X-ray Instrumentation (LEXI) of the University of California, Irvine for X-ray diffraction characterization and Mr. Allen Kine for his insightful observations. Lawrence Kulinsky and Marc Madou would like to acknowledge the support of the WCU program at UNIST as well as funding support of National Science Foundation (ECCS 0801792 and CBET 0709085) and UC Lab Fees Award 09-LR-09-117362.

References

[1] M. Gad-el-Hak, Introduction, in: M. Gad-el-Hak (Ed.), MEMS Handbook—Introduction and Fundamental, CRC Press, Boca Raton, FL, 2002 (Chapter 1, pp. 1.1–1.5/Chapter 9, pp. 9.1–9.39).
[2] C. Liu, Adv. Mater. 19 (2007) 3783–3790.
[3] J. Thaysen, A.D. Yalcinkaya, P. Vettiger, A. Menon, J. Phys. D: Appl. Phys. 35 (2002) 2698–2703.
[4] M.M. Ling, Z. Bao, Chem. Mater. 16 (2004) 4824–4840.

[5] A. Tagaya, Y. Koike, T. Kinoshita, E. Nihei, T. Yamamoto, K. Sasaki, Appl. Phys. Lett. 63 (1993) 883–884.
[6] M. Angelopoulos, IBM J. Res. Dev. 45 (2001) 57–75.
[7] R.H. Friend, R.W. Gymer, A.B. Holmes, J.H. Burroughes, R.N. Marks, C. Taliani, D.D.C. Bradley, D.A. Dos Santos, J.L. Bredas, M. Logdlund, W.R. Salaneck, Nature 397 (1999) 121–128.
[8] M. Gross, D.C. Muller, H. Nothofer, U. Scherf, D. Neher, C. Brauchle, K. Meerholz, Nature 405 (2000) 661–665.
[9] J.A. Morales, S.J. O'Sullivan, J.F. Cassidy, Sens. Actuators B 105 (2005) 266–270.
[10] S. Kirchmeyer, K. Reuter, J. Mater. Chem. 15 (2005) 2077–2088.
[11] L.B. Groenendaal, F. Jonas, D. Freitag, H. Pielartzik, J.R. Reynolds, Adv. Mater. 12 (2000) 481–494.
[12] J. Huang, P.F. Miller, J.C. de Mello, A.J. de Mello, D.D.C. Bradley, Synth. Met. 139 (2003) 569–572.
[13] http://www.clevios.com/.
[14] S.M. Richardson-Burns, J.L. Hendricks, B. Foster, L.K. Povlich, D. Kim, D.C. Martin, Biomaterials 28 (2007) 1539–1552.
[15] D. Svirskis, J. Travas-Sejdic, A. Rodgers, S. Garg, J. Control. Release 146 (2010) 6–15.
[16] U. Lang, N. Naujoks, J. Dual, Synth. Met. 159 (2009) 473–479.
[17] C.M. Hassan, N.A. Peppas, Adv. Polym. Sci. 153 (2000) 37–65.
[18] C. Chen, J.C. LaRue, R.D. Nelson, Mater. Res. Soc. Symp. Proc. 1134 (2009) BB05–BB41.
[19] W.D. Callister Jr., Materials Science and Engineering an Introduction, John Wiley & Sons, New York, NY, 2009, pp. 126–129 (Chapter 6).
[20] R. Lakes, Viscoelastic Materials, Cambridge University Press, New York, NY, 2009 (Chapter 1, pp. 1–13/Chapter 9.8.2, pp. 359–361).
[21] J. Li, J. Suo, R. Deng, J. Reinf. Plastics Compos. 29 (2010) 618–629.
[22] K.E. Strawhecker, E. Manias, Chem. Mater. 12 (2000) 2943–2949.
[23] H. Okuzaki, M. Ishihara, Macromol. Rapid Commun. 24 (2003) 261–264.
[24] T.M. Chou, P. Prayoonthong, A. Aitouchen, M. Libera, Polymer 43 (2002) 2085–2088.
[25] A. Elshner, F. Jonas, S. Kirchmeyer, K. Wussow, Asia Display/IDW, Nagoya, Japan, 2001, p. 1427.
[26] W. Gindl, Keckes, J. Compos. Sci. Technol. 66 (2006) 2049–2053.
[27] T. Kitagawa, M. Ishitibi, K. Yabuki, J. Polym. Sci. Part B: Polym. Phys. 38 (2000) 1605–1611.
[28] T.Y. Kim, C.M. Park, J.E. Kim, K.S. Suh, Synth. Met. 149 (2005) 169–174.
[29] J.W. Choi, M.G. Han, S.Y. Kim, S.G. Oh, S.S. Im, Synth. Met. 141 (2004) 293–299.
[30] B. Oh, W.J. Wang, Y.M. Lee, J. Appl. Polym. Sci. 59 (1996) 227–233.